Pure Appl. Geophys. 174 (2017), 4183–4196

DOI 10.1007/s00024-017-1634-7

Pure and Applied Geophysics

On the Theory of Solitons of Fluid Pressure and Solute Density in Geologic Porous Media, with Applications to Shale, Clay and Sandstone

A. Caserta,[1] R. Kanivetsky,[2] and E. Salusti[3]

Abstract—We here analyze a new model of transients of pore pressure p and solute density ρ in geologic porous media. This model is rooted in the nonlinear wave theory, its focus is on advection and effect of large pressure jumps on strain. It takes into account nonlinear and also time-dependent versions of the Hooke law about stress, rate and strain. The model solutions strictly relate p and ρ evolving under the effect of a strong external stress. As a result, the presence of quick and sharp transients in low permeability rocks is unveiled, i.e., the nonlinear "Burgers solitons". We, therefore, show that the actual transport process in porous rocks for large signals is not only the linear diffusion, but also a solitons presence could control the process. A test of a presence of solitons is applied to Pierre shale, Bearpaw shale, Boom clay and Oznam-Mugu silt and clay. An application about the presence of solitons for nuclear waste disposal and salt water intrusions is also discussed. Finally, in a kind of "theoretical experiment" we show that solitons could also be present in higher permeability rocks (Jordan and St. Peter sandstones), thus supporting the idea of a possible occurrence of osmosis also in sandstones.

Key words: Transients in porous rocks, solitons in geologic porous media, nonlinear Burgers shock waves.

1. Introduction

Recent research of geologic porous media has revealed how semi-permeable membranes can create chemical gradients, generated by osmosis (Marine and Fritz 1981; Alexander 1990; House and Pritchett 1995; Nunn 1997; Neuzil 2000; Neuzil and Provost 2009; Hart 2012). This process occurs not only in low permeability rocks (e.g., clay, shale….), but also in limestone, dolomite and low permeability concrete. To quantify the effect of chemical gradients, Ghassemi and Diek (2003, hereafter GD03) developed non-Osanger (Onsager 1931) analytical models to describe fluid transport forced by osmosis and pore pressure unbalances around a borehole. Then, Merlani et al. (2011, MSV in the following) analyzed a nonlinear version of the GD03 equations with full consideration of advection. Among the solutions of a nonlinear version of the GD03 model, MSV found quick and sharp transients of p and ρ, the "Burgers solitons" (Whitham 1974).

The purpose of this research is to examine the evolution of p and ρ in homogeneous geologic porous media, to establish whether or not such solitons are present. The hypothesis of homogeneity of the matrix implies to disregard the natural rock variability, but allows a much simpler analysis. To address this topic, we here analyze the evolution of ρ and p in clay, shale, silt and finally sandstones to validate if solitons can occur also in these rocks.

In earlier studies of geologic porous media, solitons were cited to explain the transport of magma in the crust (Scott and Stevenson 1984; Wiggins and Spiegelman 1995), a bradysism in Campi Flegrei (Bonafede 1991) and also of fluids in sedimentary basins (Connolly and Podladchikov 1998, 2014). The occurrence of solitons indeed can support the presence of osmosis in geologic porous media, not only in low permeability deposits, but also in highly permeable rocks, such as sandstones.

In this paper, we first describe the early GD03 and MSV models (Sects. 2, 3) and in Sect. 4 we analyze the case of pressure transients strong enough to deform the matrix. We briefly analyze also the case

Electronic supplementary material The online version of this article (doi:10.1007/s00024-017-1634-7) contains supplementary material, which is available to authorized users.

[1] Istituto Nazionale Geofisica e Vulcanologia, Rome, Italy. E-mail: arrigo.caserta@ingv.it
[2] Department of Bioproducts and Biosystems Engineering, University of Minnesota, 1390 Eckles Ave, St. Paul, MN 55108, USA.
[3] INFN Sezione, Roma 1, piazzale A. Moro 5, 00185 Rome, Italy.

of long-time clay consolidations. A completely novel viewpoint is, therefore, presented in this paper, considering nonlinear effects such as advection, rock deformation due to a large pore pressure or time-delayed clay consolidations. In Sects. 5, 6, 7, 8, 9 and 10, we present the applications of our model to Pierre shale, Bearpaw shale, Boom clay and Oxnard-Mugu silt and clay. Finally, we use our model in Sect. 11 to determine the possible occurrence of solitons, i.e., revealing osmosis phenomena in sandstones.

2. The Early Models

Analysis of transients in porous rocks is a classical problem. Rice and Cleary (1976) analyzed the transport processes in homogeneous porous media with a linear model of isothermal pressure transients. Mc Tigue (1986) added the temperature T to the above model. In a further development, Bonafede (1991) used a similar model for the analysis of waves of p and T in homogeneous porous rocks. Natale and Salusti (1996) analyzed nonlinear effects due to convective transport in these models.

The conceptual model considered in this study is that of GD03 concerning equations which describe the isothermal evolution of ρ and p, but in the nonlinear version of MSV. We indeed investigate the isothermal case of one pollutant dissolved in the fluid, with density ρ, in geologic systems where temperature gradients do not play a critical role.

In this context, Mc Tigue (1986) demonstrated that in 1-D problems the stress σ_{ij} is constant in homogeneous rocks, a fundamental assumption. The property of rock homogeneity allows simplified computations, while the effect of a realistic rock heterogeneity implies a much more complex 3-D analysis, where also the stress plays a role. In addition, it is only in such 1-D context that MSV obtained an equation relating 1-D gradients of p and ρ in homogeneous rocks, i.e., our first equation

$$\frac{\partial p}{\partial t} + E\frac{\partial \rho}{\partial t} + F\frac{\partial^2 p}{\partial x^2} + H\frac{\partial^2 \rho}{\partial x^2} = 0 \qquad (1)$$

where we call $E = -\frac{\omega_0}{\alpha^2 + KV}\left(\frac{1}{\bar{\rho}} - \frac{1}{\bar{\rho}_D}\right) \approx -10^5$, $H = \frac{k\,\Theta\,\bar{\rho}_f R^* T K}{\mu\, M^S(\alpha^2 + KV)}\left(\frac{1}{\bar{\rho}_D} + \frac{1}{\bar{\rho}}\right) \approx 10^3$ and $F = -\left(\frac{k}{\mu}K + \frac{k\,\Theta\,K\,\bar{\rho}_f}{\mu\,\bar{\rho}_D}\right)/(\alpha^2 + VK) \approx -10^{-5}$ in SI.

In Eq. (1) $\bar{a}$ is the average of a, k is the intrinsic permeability, μ is the fluid viscosity, Θ is the standard solute reflection coefficient ($0 < \Theta < 1$, GD03), K is the bulk modulus, R^* is the universal gas constant, α is the Biot coefficient, ρ_D is the solvent density $\approx$ 1000 in SI, ρ_f is the fluid density, ω_0 is the swelling coefficient, K_s is the bulk modulus of the solid matrix, K_f the fluid bulk modulus, D is the solute diffusion coefficient, φ is the rock porosity, $V = \frac{\alpha - \phi}{K_s} + \frac{\phi}{K_f} - \frac{\omega_0}{K}\frac{M^S}{R^* T \bar{\rho}_D}$ and M^S is the molar mass of the solute, often NaCl.

In (1), the parameter $H/E \approx -10^{-8}$ in SI is the solute diffusion coefficients if T and p are constant, $F \approx -10^{-5}$ in SI is the classical pressure diffusion coefficient. In the following, we moreover show that—$E \approx 10^5$ in SI is the ratio between pressure and solute density, i.e., the two components of a transient.

Equation (1) essentially relates variations of ρ and p in isothermal processes. In more detail, if a process has no initial gradients of pressure, or solute, then in (1) the system evolution is only described by the classical diffusion equation. However, in the presence of gradients of ρ and p the result is a transient of both these quantities strictly related in their concomitant evolution.

Following GD03 and MSV, our second equation is the solute mass conservation

$$\frac{\partial \rho}{\partial t} + M\frac{\partial p}{\partial x}\frac{\partial \rho}{\partial x} + N\left(\frac{\partial \rho}{\partial x}\right)^2 + S\frac{\partial^2 \rho}{\partial x^2} + U\frac{\partial^2 p}{\partial x^2} = 0 \qquad (2)$$

where in SI we have $M = -\frac{k}{\phi\,\mu}\left[\frac{1}{\bar{\rho}_f} + \frac{\Theta}{\bar{\rho}_D}\right]\bar{\rho}_f \approx -10^{-12}$ $N = \frac{k}{\mu\phi}\Theta\frac{R^* T}{M^S}\left[\frac{1}{\bar{\rho}_D} + \frac{1}{\bar{\rho}}\right]\bar{\rho}_f \approx -10^{-12}$ $S = -\frac{D}{\phi} \approx -10^{-18}$ and $U = \frac{M^S D\,\bar{\rho}}{R^* T\,\phi\,\bar{\rho}_f} \approx 10^{-14}$.

In (2), the "nonlinear" parameters M (if p is not constant) and N (for constant p) determine the effect of advection while S is the solute diffusion parameter if p is constant. Tables 1 and 2 also demonstrate the intrinsic relation

$$F/H = M/N \qquad (3)$$

of importance to simplify some formulas.

As initial/boundary conditions in the above studies are often considered a fluid saturated porous-permeable homogeneous rock (for $x < 0$,

Table 1

Estimated values of relevant rock parameters in SI

Parameters	Pierre shale	Bearpaw shale	Boom clay	Oxnard-Mugu silt and clay	St. Peter sandstone	Jordan sandstone	Units
Rock porosity (φ)	0.3	0.4	0.4	0.36	0.27	0.31	–
Intrinsic permeability (k)	10^{-18}	5×10^{-21}	5×10^{-18}	10^{-16}	5×10^{-14}	5×10^{-12}	m^2
Solute reflection coefficient (Θ)	0.25	0.25	0.3	0.15	0.2β	0.2 β	–
Solute diffusion coefficient (D)	10^{-8}	5×10^{-10}	4×10^{-6}	10^{-8}	4×10^{-7}	2×10^{-9}	m^2/s
Solute molar mass (M^s) (NaCl)	0.06	0.06	0.06	0.06	0.06	0.06	kg/mol
Biot coefficient (α)	0.7	0.6	0.6	0.45/0.63	0.5	0.5	–
Swelling coefficient (ω_0)	10^5	2×10^6	5×10^5	2×10^5	$10^5\beta$	$8 \times 10^4\beta$	Pa
Bulk modulus (K)	4×10^6	4×10^6	8×10^6	10^7	2×10^7	2×10^7	Pa
Bulk modulus of the matrix (K_s)	10^7	1.5×10^7	2×10^7	2×10^7	4×10^7	2.2×10^9	Pa
Estimated solute density ($\bar{\rho}$)	1	16/33	5	1.34–1.92	0.25–0.5	0.5	kg/m^3
Estimated pore pressure (p)	10^5	2.4×10^5	2×10^5	3×10^5	3×10^5 β	$4 \times 10^5\beta$	Pa

In addition to this table, the quantities discussed in the text are the fluid viscosity $\mu \approx 3 \times 10^{-5}$, ρ the solute intrinsic mass fluid density; the solvent fluid intrinsic mass density $\rho_D \approx 10^3$ and $K_f \approx 10^9$ the fluid bulk modulus in SI

contaminant $\rho_0 + \rho^*$ and pressure $p_0 + p^*$ at $t \approx 0$) as the "source". The transient is assumed to move towards an adjacent homogeneous porous rock ($x > 0$, contaminant ρ_0 and pressure p_0 at $t \approx 0$). These initial values ρ^* and p^* will play a fundamental role in this model.

We note that Greenberg et al. (1973) obtained similar equations but with a more complex mathematical structure.

3. The "Burgers Solitons"

Assuming, as in MSV, the ansatz that

$$F\frac{\partial^2 p}{\partial x^2} + H\frac{\partial^2 \rho}{\partial x^2} = -\frac{\mathrm{d}}{\mathrm{d}t}f(t) \tag{4}$$

from (1) we obtain that $p + E\rho = f(t)$, i.e., a function of time only. Such ansatz is suggested by a mathematical analysis of Merlani et al. (2001) about symmetry properties of the Eqs. (1) and (2). It identified solutions as functions of (x^2/t), classical for diffusive phenomena, or of $(x - Ut)$ of less interest since it describes rigid translations only.MSV obtained from (1), (2) and (4) a Burgers-like equation

$$\frac{\partial \rho}{\partial t} + A\left(\frac{\partial \rho}{\partial x}\right)^2 - Z\frac{\partial^2 \rho}{\partial x^2} = 0 \tag{5}$$

calling $A = N - EM$ and $Z = UE - S$. The Reynolds number

$$\boldsymbol{R} = (2A\rho^*)/Z \tag{6}$$

is fundamental (Fig. 1) to distinguish between linear and nonlinear solutions of (5) (Whitham 1974; Caserta et al. 2013). Indeed if $\boldsymbol{R} > 8$–10 as for a strong initial density, the solution of (5) is

$$\begin{array}{ll} \rho = \rho_0 + \rho^* & x < 0 \\ \rho = \rho_0 + \frac{x^2}{4At} & x < x_B(t) < \sqrt{4A\rho^* t} \\ \rho = \rho_0 & x > x_B(t) \end{array} \tag{7}$$

for $t > t^*$ (Fig. 2). In (7) the time t^* is necessary to avoid mathematical pathologies since for $t \approx 0$ the solution of (7) diverges. On physical grounds, t^* can be seen as a small initial delay related to the arrival of a realistic transient (MSV). It is also important to note how the solute density (Fig. 2) has a front at $x = x_B(t)$ (Appendix A). The corresponding pressure for $0 < x < x_B$ and $t > t^*$ is

$$\begin{array}{ll} p = p_0 + p^* & x < 0 \\ p = p_0 - \frac{Ex^2}{4At} + \frac{EF-H}{2A}\ln\left(\frac{t}{t^*}\right) & x < x_B(t) < \sqrt{4A\rho^* t} \\ p = p_0 & x > x_B(t) \end{array} \tag{8}$$

as a strict consequence of (4). In turn the Darcy fluid velocity is (Fig. 3)

Table 2

Numerical values of coefficients in Eqs. (1) and (2) according to estimate in Table 1, in SI

Coefficient	Pierre Shale	Bearpaw Shale	Boom Clay	Oxnard-Mugu silt and clay	St. Peter sandstone	Jordan sandstone	Units
$E = \dfrac{-\dfrac{\omega_0}{\alpha^2 + KV}}{\left(\dfrac{1}{\bar{\rho}_S} - \dfrac{1}{\bar{\rho}_D}\right)}$	-1.5×10^5	-3×10^5	-2×10^5	-2×10^5	-10^7	-10^6	m^2/s
$F = -\left(\frac{k}{\mu}K + \frac{k\Theta K\bar{\rho}_f}{\mu\bar{\rho}_D}\right)\Big/(\alpha^2 + VK)$	-2.5×10^{-8}	-2×10^{-10}	-3×10^{-7}	-10^{-5}	$-\beta\ 10^{-4}$	$-\beta\ 0.01$	m^2/s
$H = \dfrac{k\ \Theta\bar{\rho}_f R^*TK}{\mu M^S(\alpha^2\ +\ KV)\left(\dfrac{1}{\bar{\rho}_D} + \dfrac{1}{\bar{\rho}_S}\right)}$	0.2	7×10^{-5}	0.8	4	1.5×10^{-5}	7×10^{-6}	m^4/s
$M = -\frac{k}{\phi\mu}\left[\frac{1}{\bar{\rho}_f} + \frac{\Theta}{\bar{\rho}_D}\right]\bar{\rho}_f$	-10^{-14}	-5×10^{-17}	-5×10^{-14}	-10^{-12}	$-\beta\ 10^{-9}$	$-\beta\ 5 \times 10^{-8}$	$m^2/s\ Pa$
$N = \frac{k}{\mu\phi}\Theta\frac{R^*T}{M^S}\left[\frac{1}{\bar{\rho}_D} + \frac{1}{\bar{\rho}_S}\right]\bar{\rho}_f$	10^{-7}	10^{-11}	10^{-7}	10^{-6}	10^{-2}	0.5	$m^4/s^3\ Pa$
$S = -\frac{D}{\mu}$	-3×10^{-8}	-10^{-9}	-10^{-5}	-3×10^{-8}	-10^{-6}	-6×10^{-9}	m^2/s
$U = \frac{M^S D\bar{\rho}_S}{R^*T\phi\bar{\rho}_f}$	7.5×10^{-16}	7.5×10^{-16}	10^{-12}	7×10^{-16}	2×10^{-14}	$2\ \times 10^{-16}$	s
$V = \dfrac{\alpha - \phi}{K_s} + \dfrac{\phi}{K_f} - \dfrac{\omega_0}{K}\dfrac{M^S}{R^*\,T\,\bar{\rho}_D}$	2.5×10^{-8}	1.5×10^{-8}	10^{-8}	7×10^{-9}	6×10^{-9}	5×10^{-9}	Pa^{-1}

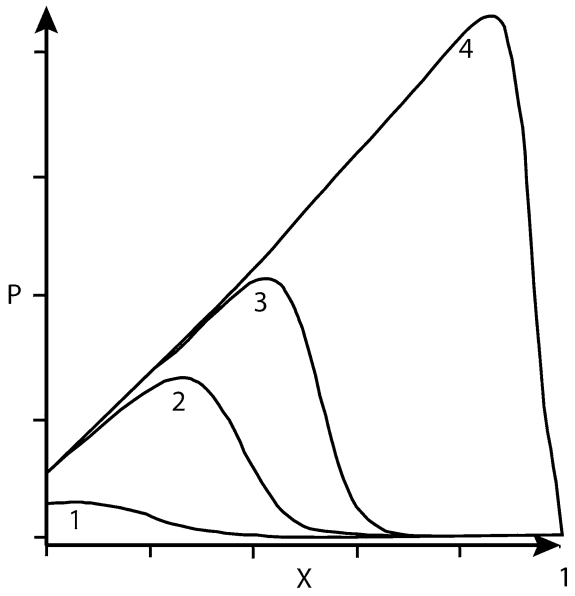

Figure 1
Qualitative sketch of the solutions of Burgers equation, with $\boldsymbol{R} = 1$ for curve 1; $\boldsymbol{R} = 5$ for curve 2; $\boldsymbol{R} = 9$ for curve 3; $\boldsymbol{R} = 25$ for curve 4

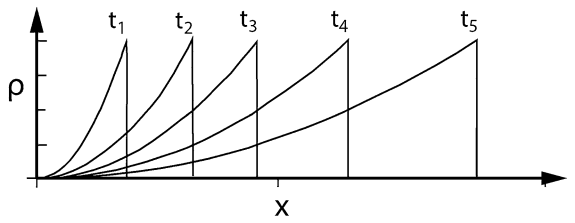

Figure 2
Intuitive sketch of the variation of ρ with distance at different increasing times

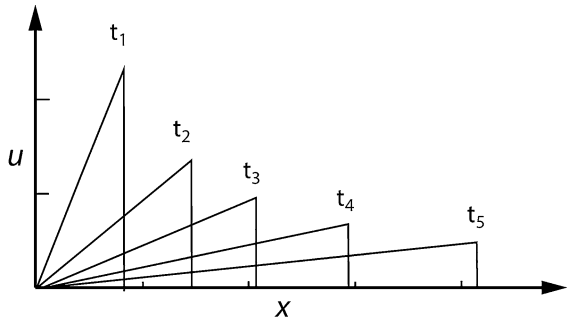

Figure 3
Intuitive sketch of the variation of $u(x, t)$ with distance at various increasing times

$$u_{\mathrm{D}} = -\frac{k}{\mu\phi}\frac{\partial p}{\partial x} = \frac{Ek}{\phi\mu}\frac{\partial \rho}{\partial x} \tag{9}$$

where k, μ…. are in Table 1. We also note how the pressure has a component $\frac{EF-H}{2A}\ln\left(\frac{t}{t^*}\right)$ that somehow reminds the formulation of Sorek (1996), is rather small, has no effect on the fluid velocity, is difficult to be related to physical effects and in the following will be disregarded.

In comparison with the usual diffusion front velocity $\sqrt{4\pi D/t}$, the nonlinear front velocity is $\sqrt{A\rho^*/t}$ if $\boldsymbol{R} > 8$–10.

Since $\boldsymbol{R}$ depends also from the initial density jump ρ^*, it can be very large for large initial conditions p^* or ρ^*. On practical grounds, ρ^* can therefore play a fundamental role, also to reveal if in a given rock can occur a low classical diffusion or a quick solitons related to osmosis.

It is moreover important to stress how the ansatz (4) is verified in the solutions (7) and (8).

The parameters E, F…, U, A and Z are rather poorly known quantities and therefore they must be considered critically, as discussed in the Appendix B.

4. The Effect of Generalized Hooke Relations: Large Initial Pressure and Time Variability

4.1. Large Initial Pressure

We now discuss the case of a large initial pressure: in Eq. (1) we consider a pressure $p \to \Phi(p) = p + \eta^* p^2$ with a quadratic correction of the linear "Hooke law" of GD03. This η^* could be very small for elastic or brittle behaviors but for a ductile zone $\eta^* < 0$, which must simulate the profile of Fig. 4.

The equations of the novel model, therefore, are

$$\begin{cases} E\dfrac{\partial \rho}{\partial t} + \dfrac{\partial \Phi(p)}{\partial t} + F\dfrac{\partial^2 p}{\partial x^2} + H\dfrac{\partial^2 \rho}{\partial x^2} = 0 \\ \dfrac{\partial \rho}{\partial t} + M\dfrac{\partial p}{\partial x}\dfrac{\partial \rho}{\partial x} + N\left(\dfrac{\partial \rho}{\partial x}\right)^2 + S\dfrac{\partial^2 \rho}{\partial x^2} + U\dfrac{\partial^2 p}{\partial x^2} = 0 \end{cases} \tag{10}$$

To check if the terms in S and U can be again disregarded in comparison with the nonlinear terms, we repeat the previous estimate and find that

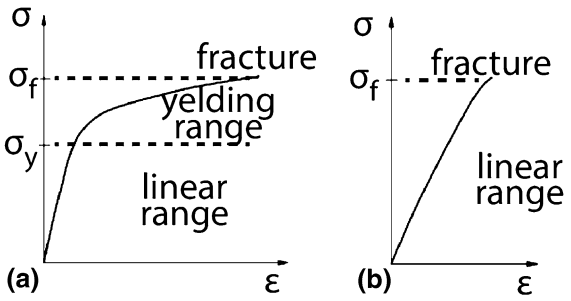

Figure 4
Two typical stress–strain curves are schematically shown: **a** ductile behavior and **b** brittle behavior, for materials under uniaxial tension

$\boldsymbol{R_{nl}} = \frac{N\left(\frac{\partial \rho}{\partial x}\right)^2 - M E \frac{\partial \Phi(\rho)}{\partial x}\frac{\partial \rho}{\partial x}}{S\frac{\partial^2 \rho}{\partial x^2} - E U \frac{\partial^2 \rho}{\partial x^2}} \approx N\rho/S$ plays a role similar to $\boldsymbol{R}$ in (5), and thus we will again disregard S and U if $\boldsymbol{R_{nl}} > 8$–10 (Whitham 1974).

To solve the system (10), we assume $p = \Gamma(\rho) + X$ for a yet undetermined but very general function X, as somehow suggested by (4). From the second equation of (10), we thus have

$$\frac{\partial \rho}{\partial t} + M\frac{\partial [\Gamma(\rho) + X]}{\partial x}\frac{\partial \rho}{\partial x} + N\left(\frac{\partial \rho}{\partial x}\right)^2 = \frac{\partial \rho}{\partial t} + \left[N\frac{\partial \rho}{\partial x} + \frac{M\partial [\Gamma(\rho) + X]}{\partial \rho}\right]\frac{\partial \rho}{\partial x} \approx 0 \tag{11}$$

for a large $\boldsymbol{R_{nl}}$. By multiplying this (11) for $N + M\frac{\partial}{\partial \rho}[\Gamma(\rho) + X)]$ we obtain the solution

$$N\rho + M[\Gamma(\rho) + X] = N\rho + Mp = \frac{x^2}{4t} + \cos t \tag{12}$$

By replacing this (12) in (10) and applying (3), one finally obtains

$$-\frac{EM}{N}\frac{\partial p}{\partial t} + \frac{\partial \Phi(p)}{\partial t} + \frac{Ex^2}{4Nt^2} + F\frac{\partial^2 p}{\partial x^2} + H\frac{\partial^2 \rho}{\partial x^2} = -\frac{EM}{N}\frac{\partial p}{\partial t} + \frac{\partial \Phi(p)}{\partial t} + \frac{Ex^2}{4Nt^2} + \frac{2H}{Nt} = 0 \tag{13}$$

In this way, the cumbersome system (10) becomes just a simple equation. Its solution is

$$p^2 + Ap/\eta^* N + Ex^2/4\eta^* N t = (2H/N\eta^*)\ln(t/t^*) \tag{14}$$

Disregarding again the small term with $(2H/N\eta^*)\ln(t/t^*)$, we approximately obtain

$$p \approx -\frac{Ex^2}{4At} - \frac{\eta^* E^2 N}{16A}\frac{x^4}{t^2} + \ldots\ldots \tag{15}$$

Since $\eta^* < 0$, the first-order correction for a large pressure input, therefore, is a pressure increase

$$-\frac{\eta^* E^2 N}{16A}\frac{x^4}{t^2} \tag{16}$$

We also remark how often in these rocks $N \approx A \approx 10^{-7}$ in SI, while $E \approx -10^5$ (Tables 1, 2) and, therefore, we approximately obtain

$$p \approx -\frac{Ex^2}{4At} - \frac{\eta^* E^2}{16}\frac{x^4}{t^2} + \cdots \approx 10^{12}\frac{x^2}{t} - 10^8\eta^*\frac{x^4}{t^2}\ldots\ldots\ldots \tag{17}$$

which shows the importance of η^* for short times.

This assumption $p \to \Phi(p) = p + \eta^* p^2$ can, however, give only a partial response to rock deformation processes since the concomitant evolution of porosity and permeability can play a relevant role. On the other hand, it is known that φ and k are remarkably pressure dependent (Bonafede 1991; Shapiro and Dinske 2009). Therefore, the comparison between these two approaches can be seen as an interesting open question for future studies.

4.2. Time-Dependent Hooke Law

In the preceding analyses, we consider a time independent Hooke relation, but in many overconsolidated clays the stress–strain relation is strongly time dependent (Yin and Graham 2011; Lerouel et al. 1985). Indeed significant time-delayed consolidations are evident in clays, often seen as various steps of the whole clay consolidation process. All of this has an important practical application, for example for sequestration of CO_2 or radioactive waste disposal (Erol 1977; Fabre and Pellet 2006).

Among many models proposed for practical application, Lerouel et al. (1985) in the version of Yin and Graham (2011) is somewhat similar to our model. Indeed, in a generalized Hooke law they consider also the effect of a time-dependent strain "rate", i.e., the time derivative of the volume

fraction, here expressed as a linear combination of p and ρ (GD03, MSV). We can, therefore, analyze a stress–strain–rate relation as the origin of some subsequent clay consolidations. Thus, the novel version of our Eq. (10) is

$$\begin{cases} E\dfrac{\partial \rho}{\partial t}+\dfrac{\partial p}{\partial t}+m\dfrac{\partial^2 p}{\partial t^2}+n\dfrac{\partial^2 \rho}{\partial t^2}+F\dfrac{\partial^2 p}{\partial x^2}+H\dfrac{\partial^2 \rho}{\partial x^2}=0 \\ \dfrac{\partial \rho}{\partial t}+M\dfrac{\partial p}{\partial x}\dfrac{\partial \rho}{\partial x}+N\left(\dfrac{\partial \rho}{\partial x}\right)^2+S\dfrac{\partial^2 \rho}{\partial x^2}+U\dfrac{\partial^2 p}{\partial x^2}=0 \end{cases} \tag{18}$$

To analyze the solutions of (18), we here discuss a simple solution, assuming m and n constant and $\rho = x^2\, r(t)$ and $p = x^2\pi(t)$, as suggested by (4). Then, from (18) we have

$$\begin{cases} E x^2\dfrac{\mathrm{d}\,(r+n\frac{\partial r}{\partial t})}{\mathrm{d}\,t}+x^2\dfrac{\mathrm{d}\,(\pi+m\frac{\partial \pi}{\partial t})}{\mathrm{d}\,t}+2F\pi \\ \quad +2Hr=0 \\ x^2\dfrac{\mathrm{d}\,r}{\mathrm{d}\,t}+4Mx^2\dfrac{\mathrm{d}\,\pi}{\mathrm{d}\,t}\dfrac{\mathrm{d}\,r}{\mathrm{d}\,t}+4Nx^2\left(\dfrac{\mathrm{d}\,r}{\mathrm{d}\,t}\right)^2+2Sr \\ \quad +2U\pi=0 \end{cases} \tag{19}$$

This in turn implies that the solution describing the arrival of a p and ρ transient in clays is

$$\begin{cases} E\dfrac{\mathrm{d}\,(r+n\frac{\partial r}{\partial t})}{\mathrm{d}\,t}+\dfrac{\mathrm{d}\,(\pi+m\frac{\partial \pi}{\partial t})}{\mathrm{d}\,t}=0 \\ 4M\dfrac{\mathrm{d}\,\pi}{\mathrm{d}\,t}+4N\dfrac{\mathrm{d}\,r}{\mathrm{d}\,t}=0 \end{cases} \tag{20}$$

and consequently $Er + En\ \mathrm{d}r/\mathrm{d}t + \pi + m\ \mathrm{d}\pi/\mathrm{d}t = \mathrm{const}'$ and $M/N\,\pi + r = \mathrm{const}''$. This finally gives that the solutions $\pi(t)$and $r(t)$ are just time exponentials for m and n constants.

In the following, we apply these ideas to low permeability geologic rocks, generalizing an early study about Perre shales (Caserta et al. 2013).

5. Pierre Shale

The Pierre shale is a low permeability formation of Upper Cretaceous age. This dark-gray shale is fossiliferous, has maximum thickness of about 210 m and overlies sandstone aquifer systems (Bredehoeft 1983). The Pierre shale is correlated with other marine shales that occur farther west, such as the Bearpaw shale in United States and Canada (Caserta et al. 2013). The data discussed in Table 1 were obtained in central South Dakota, USA (Barbour and Fredlund 1989; Neuzil 2000; Simm 2007; Neuzil and Provost 2009; Sarout and Detournay 2011). Its mineralogy is 70–80% of clay, of which about 80% is a mixed layer of smectite-illite. The shale, at this site, is saturated at the depth of $\sim$75 m.

To estimate the swelling coefficient ω_0, we compare the Sarout and Detournay (2011) with GD03 articles and obtain an average value $\omega_0 \approx 10^5$ Pa. The other data in the Table 2 show that for Pierre shales $A = N - M$ $E \approx 10^{-7}$ and $Z = EU - S \approx 3 \times 10^{-8}$ in SI (Tables 1, 2). This gives a small $\boldsymbol{R} \approx 3\rho^*$; therefore, solitons can be present if initially $\rho^* > 3$ in SI, or equivalently the initial pressure $p^* > 10^6$ in SI.

Since $\eta^* < 0$, a strong initial pressure implies a positive pressure variation as large as $-\frac{\eta^* E^2 N}{16\,A}\frac{x^4}{t^2} \approx -10^8\,\eta^*\frac{x^4}{t^2}$.

6. Bearpaw Shale

The Bearpaw Formation, also called the Bearpaw shale, is a sedimentary rock found in Northwest Saskatchewan, east of the Rocky Mountains. To the east and south it blends into the Pierre shale. The data reported here were measured near Saskatoon, Saskatchewan, Canada (Cey et al. 2001). This site consists of a $\sim$76 m thick, massive and plastic marine clay (about 5% sand, 38% silt and 57% clay) deposited approximately 70 million years before present, at a depth of about 88–123 m.

The mineralogy of the Bearpaw shale is claystone, somehow similar to Pierre shale but with total clay of $\sim$57%, of which 50–60% is smectite with lesser amount of illite (10–20%). Indeed Pierre shale and this Bearpaw shale are somehow similar rocks from a mineralogy and origin point of view (Barbour and Fredlund 1989; Cey et al. 2001; Simm 2007; Neuzil and Provost 2009). Therefore, some not well-known values are tentatively assumed to be as those of Pierre shale.

From Tables 1 and 2 for an average solute density ≈ 25 kg/m^3 in the Bearpaw shale, we have $A = N - M\ E \approx 3 \times 10^{-11}$ and $Z = EU - S \approx 10^{-9}$ in the SI and thus $\boldsymbol{R} \approx 3\ \rho^* 10^{-2}$.

To have a soliton, it is therefore necessary to have a very large value $\rho^* \approx 300$, much larger than that of Pierre shale.

All of this implies that if a waste disposal facility placed in Bearpaw shale would enter in contact with some external fluid, a larger impact of pressure in comparison with those for the Pierre shale is necessary to generate large and quick transients.

For a strong initial pressure, one has again a positive jump

$$-\frac{\eta^* E^2 N}{16\ A}\ \frac{x^4}{t^2} \approx -10^8\, \eta^* \frac{x^4}{t^2}. \qquad (21)$$

7. Boom Clay

The Oligocene Boom clay is silty clay of marine origin occurring in north-eastern Belgium. It is plastic clay (19–26%) with total porosity of 0.35–0.40. The average clay mineral content (phyllo-silicates) is 60% water in weight and the clay mineralogy is dominated by illite/smectite mixed layers with a detail mineralogy of clay 30–70%, smectite 10–30%, mixed layer smectite-illite 5–50%, illite 10–30%, and chlorite 1–5% (Helgerud et al. 1999; Garavito et al. 2007; Neuzil and Provost 2009; Delage et al. 2010).

From the values in Table 2 we obtain $A = N - EM \approx 10^{-7}$ and $Z = EU - S \approx 10^{-5}$ and, therefore, $\boldsymbol{R}$ is about 0.01 ρ^*. Also in this case shock solitary waves are possible, but for a very large initial $\rho^* \approx 10^3$ or an external pressure p^* about 10^7 in SI. One can, therefore, have Burgers solitons, but for very large values of ρ^*. All of this implies that if a radioactive disposal facility placed in Boom shale would be in contact with some external fluid, in comparison with those for the Pierre shale a really larger impact of pollutants would be necessary to generate such transients (Henrion et al. 1990).

Again a strong initial pressure implies a positive variation very similar to those already found for Pierre shale $-\frac{\eta^* E^2 N}{16\ A}\ \frac{x^4}{t^2} \approx -10^8\, \eta^* \frac{x^4}{t^2}$.

8. Underground Waste Isolation in the Boom Clay

Clay-rich deposits are usually considered to be good natural media for underground waste isolation because of their low permeability (Garavito et al. 2007). In the absence of water conductive features, these deposits provide the environment required for a fully reliable waste containment. Indeed in these deposits the diffusion seems to be the dominant transport process because clay minerals retard the movement of contaminants by ion exchange, sorption and ultra-filtration (De Cannière et al. 1996; Cey et al. 2001). The clay deposits in the total absence of fluid conductive features are, therefore, key barrier for ensuring the long-term safety of a disposal system. In more realistic situations where some amount of water is present, the comprehensive understanding of the physical and chemical processes controlling the water and solute transport through low permeability clay type formations is a key step for assessing their suitability as host rocks (Garavito et al. 2007).

Example of such host rock is an overconsolidated marine Oligocene deposit, the Boom Clay (Garavito et al. 2007). In addition, it is often considered as a reference host formation for waste disposal in Belgium because of its favorable characteristics. Indeed extensive hydraulic, geo-mechanical and geo-chemical research has been carried out for more than 25 years on the Boom Clay at the HADES Underground Research Laboratory (URL) in Mol (Belgium). The primary objectives of these experiments have been to characterize the in situ hydrogeological conditions, to determine the hydraulic parameters and to study the mechanisms controlling the chemistry and the composition of the Boom Clay pore water (Baeyens et al. 1985; Henrion et al. 1990; De Cannière et al. 1996).

In situ data shown in Tables 1 and 2, however, confirm the occurrence of some chemical osmosis in low permeability plastic formations, such as those present in the Boom Clay. The osmotic efficiency of Boom Clay is high under undisturbed chemical conditions, but rapidly decreases when the dissolved salts concentration increases. The semi-permeable membrane behavior of the high efficiencies Boom Clay is actually considered most important for waste disposal.

In such complex situation, our model is directly applicable to waste isolation in underground controlled facilities. The rocks under consideration for repositories must indeed have extremely low permeability and to avoid complex thermal effects the convective heat transfer must be minimal. If the temperature changes at short distance away from a heat-producing waste canister are small, the assumption of constant material properties may be considered as appropriate.

We now test the flexibility of our model with a theoretical simulation, i.e., we compute the variations of Table 1 as if the solute in Boom Clay is not the usual NaCl but a material with a larger solute molar mass, say, $M^s = 0.18$, to simulate dangerous nuclear waste as Cesium 137 clorure. This could somehow simulate the eventual propagation of rather heavy, soluble material when in contact with the deposit boundary. We also tentatively assume the same increase of about 300% for the values of the solute density and solute reflection coefficient, following the assumption that such coefficients may follow the solute molar mass increase while the permeability k and the diffusion D can be considered inversely dependent, for the same 300% estimated value (not shown).

With these heuristic estimates we find that $A = N - EM \approx 2 \times 10^{-8}$ and $Z = EU - S$ is about 2×10^{-6} and, therefore, A/Z is as small as ≈ 0.02 and also $\boldsymbol{R}$ is a small $\approx 0.02\ \rho^*$. Also in this case shock solitary waves are possible in this model, but for a very large initial stress $\rho^* \approx 5 \times 10^2$ or an external pressure stress $p^* \approx 10^8$. This confirms the wise choice of this kind of rock for deep nuclear deposit.

9. Oxnard-Mugu Silt and Clay

The late Pleistocene Oxnard-Mugu silt and clay deposits occur in Oxnard coastal basin, Ventura County (California). A confining bed, consisting of silt and clay, separates the Oxnard and Mugu aquifers. These sediments have maximum thickness of 46 m, are well stratified and the strata are composed mainly of silty material. The lateral extent of these rocks is approximately 20–30 km (California Department of Water Resources 1971).

Laboratory investigation of the pore fluids in such silt and clay strata (Greenberg et al. 1973) indicated NaCl concentrations of 1.3/1.9 and in our analysis we thus assume the average $\rho \approx 1.6$. Coupled salt and water flows have indeed been observed through this low permeability material (i.e., the confining bed, consisting of silt and clay), but no detail mineralogy is studied (Delage et al. 2010; Helgerud et al. 1999). Since some detailed mineralogy for this basin is not available, we heuristically assume for α and Θ an average of the same values provided for shales and clays.

The values of Table 2 give $A = N - ME \approx 10^{-6}$ and $Z = S - E\ U \approx 3 \times 10^{-8}$ and, therefore, the corresponding $\boldsymbol{R} \approx 10^2 \rho^*$. In these rocks, one can easily have cases of solitary waves also for small values of ρ^*. A strong initial pressure again gives a similar positive variation $-\frac{\eta^* E^2 N}{16\,A}\ \frac{x^4}{t^2} \approx -\ 10^8\, \eta^* \frac{x^4}{t^2}$.

10. Sea Water Intrusion in the Oxnard Coastal Basin

The groundwater structure in the Oxnard coastal basin is a multiple aquifer system of successive confining beds and aquifers, described by Greenberg et al. (1973). The Oxnard aquifer, which is at a depth of about 49 m and was the principal producing aquifer in the basin, has been intruded since years 1930 by seawater because of a general lowering of groundwater levels. This seawater intrusion, which now extends several miles inland, poses a serious threat to the water resources of the region since the Oxnard aquifer has been the principal source of water for the Oxnard area.

Where water from the Oxnard can no longer be used because of the seawater intrusion, wells have been drilled to the deeper Mugu aquifer, which is separated from the Oxnard by an aquitard layer of fine-grained material. The possible consequences of the seawater diffusion are discussed by Greenberg et al. (1973), and are:

1. the above salt intrusion, since $E < 0$, gives a pressure increase in the aquifer and in turn a consolidation of the aquitards. This can lead to

surface subsidence since in this basin the coefficient of compressibility is $a_v \approx 3.5 \times 10^{-6}$ in SI. Bonafede (1991) discussed similar phenomena in connection with the bradyseismic crisis in the CampiFlegrei.

2. the increase of NaC1 concentration in the Oxnard aquifer would tend to drive NaCl into and through the adjacent aquitard by diffusion or advection. Thus, NaCl would contaminate adjacent aquitard and the contiguous Mugu aquifer.

To review the above points, we state that the presence of the marine salt in the upper layer, with a density $\rho^* \sim 1.6$, gives a very large $\boldsymbol{R} \sim 400$. Our model thus can allow a tentative forecast, since the geological properties of the basin allow the presence of transients of salt density: a rather sharp and quick movement of marine salt can probably take place in these basins.

11. A "Theoretical Experiment" About Osmosis in Sandstones

Our model can be tentatively applied to rocks where osmosis has not yet been measured but could potentially occur, following Alexander (1990), Neuzil and Provost (2009), Hart (2012) among others. We, therefore, focus on effects revealing its eventual presence in St Peter Sandstone and Jordan Sandstone. We consider their ω_0 and Θ to be β times the values already found for shales. Then, we analyze the new model and its solutions to check if a possible presence of solitons could reveal osmotic properties also in sandstones.

11.1. St. Peter Sandstone

The St. Peter Sandstone is an Ordovician formation. The formation spans north–south from Minnesota to Missouri and east–west from Illinois into Nebraska in the Midwest of United States. The data discussed here (Tables 1, 2) were obtained from the regional studies in Minnesota, USA (Kanivetsky 1978; Kanivetsky and Walton 1979; Freeze and Cherry 1979). This sandstone consists of massive, fine-to-medium-size, well-rounded quartz grains, well sorted and friable, saturated at 50–60 m depth (Kanivetsky 1978; Kanivetsky and Walton 1979). Its mineralogy is of almost pure Quartzite.

From Tables 1 and 2, we obtain for St. Peter Sandstone a small $A = N - EM \approx 10^{-7} - \beta/100 \approx 10^{-7}$ in SI for a small β and again a small $Z = EU - S \approx 10^{-6}$. This gives $R \approx \beta\rho^*/10$ and this shows that solitons can be present for a large initial $\rho^* > 100/\beta$ in SI.

11.2. Jordan Sandstone

The late Cambrian Jordan Sandstone Formation is composed of a white to yellow, quartzose, fine- to coarse-grained sandstone, varying from friable to well cemented. The Jordan Sandstone is one of the major sources of groundwater in the Midwest and its extension is similar to that of St. Peter Sandstone. The mineralogy of these rocks is dominated by quartz (90% in weight). The sandstone is saturated at 70–80 m depth. The data discussed here were again obtained in Minnesota (Kanivetsky 1978; Kanivetsky and Walton 1979; Freeze and Cherry 1979).

From Tables 1 and 2 for Jordan Sandstone, we have $A = N - EM \approx 0.5 - 0.5 \quad \beta \approx 0.5$ and $Z = EU - S \approx 6 \times 10^{-9}$ while $\boldsymbol{R} \approx \beta\,\rho^* 10^8$. Following Alexander (1990), Neuzil (2000), Neuzil and Provost (2009) among others, solitons can therefore be present for $\rho^* > 10^{-7}/\beta$, certainly much more frequently than in St Peter sandstone. Consequently, our "theoretical experiment" confirms that in sandstones one can find shock solitary waves. It is, however, rather surprising that solitons can be present for such small β. In synthesis, these findings support the idea of some presence of osmosis also in relatively higher permeability rocks.

12. Discussion and Conclusions

In this paper, we analyze the effect of a strong external stress on the dynamics of nonlinear transients of ρ and p in geologic porous media, under the local action of pore pressure and osmosis. In particular, we first focus on the role of advection in low permeability homogeneous rocks. We thus obtain a nonlinear model (i.e., two equations in 1-D)

describing the evolution of transients of related ρ and p. These nonlinear model solutions unveil the presence of quick large shocks, the "Burgers solitons" (Whitham 1974), ruled by a Reynolds number $\boldsymbol{R} = 2A\rho^*/Z$ and characterized by a sharp front.

These solutions describe transients quicker and sharper than those predicted by linear models, perturbation theories or scale analyses. In particular, since $\boldsymbol{R}$ is proportional to ρ^*, a strong initial stress is needed to obtain that $\boldsymbol{R} > 8$–10, i.e., the necessary condition for the presence of solitons (Whitham 1974; Fig. 1).

This model is then applied to low permeability rocks, where osmosis is known to play an important dynamical role. In this way, we can compute the initial stress necessary to have solitons, the Reynold number $\boldsymbol{R}$, the front velocity for Pierre shale, Bearpaw shale, Boom shale, Oxnard-Mugu silt and clay.

On more practical grounds, our model moreover allows also a quick estimate of an eventual soliton transports in porous media. Indeed when we computed $\boldsymbol{R}$ for the various shales and clays, we also found a surprising large $\boldsymbol{R}$ variability in rocks that are usually considered to be similar, from about 100 ρ^* to about $\rho^*/100$. But we also observed that $\boldsymbol{R}$ is roughly proportional to just the ratio of permeability over diffusivity k/D. Such k/D is a function of the rock origin, depositional environment and subsequent evolution among other porous media, and is not related to any model characteristics. Thus, one can have a first quick estimate whether or not solitons can probably be present in a given rock just from this k/D.

This kind of quick information could be of interest for a number of geological processes, including hydrocarbon migration (Appold and Nunn 2002; Joshi et al. 2012), development of epikarst environment (Dragila et al. 2016), nuclear waste disposal (Kim et al. 2011; Gonçalvès et al. 2012), borehole drilling (Zhang 2011; Zeynali 2012), CO_2 sequestration, etc……

We also discuss a "theoretical experiment" to analyze whether or notosmotic phenomena can be present in highly permeable geological porous media such as sandstones. We assume for sandstones that the swelling and solute diffusion coefficients (i.e., the main quantities related to osmosis) are as those for clay but multiplied by a small, or also very small, heuristic parameter β. In this way, we can see that rather large $\boldsymbol{R}$ can hold for Jordan and St. Peter sandstone, thus supporting the formation of solitons also in higher permeability rocks.

In conclusion, this heuristic "experiment" can allow to check if osmotic processes may also occur in fluid migration (Magara 1974), in nuclear waste disposal (Kim et al. 2011), borehole drilling (Schlemmer et al. 2003) and shale gas production (Engelder et al. 2014), despite the fact that osmotic constants and properties of geologic porous media are rather poorly understood.

In addition, some of our results give origin to open questions. The effect of a realistic rock heterogeneity is a very complex problem in 3-D and cannot be solved with this model.

In addition, when we investigate rock deformation effects we just consider a nonlinear pressure $p \to \Phi(p) = p + \eta^* p^2$ in a generalized Hooke law for strain, pressure and solute density (GD03). We obtain a pressure increase $-\frac{\eta^* E^2 N}{16\,A}\,\frac{x^4}{t^2} \approx -10^8\,\eta^*\frac{x^4}{t^2}$. But such rock deformation can also be seen as a due to a rock parameters variability, like the pressure-dependent permeability $k(p)$. The relation between these two different viewpoints remains an open question.

We also analyze the case of a time-dependent Hooke law among stress, strain and their rates (Lerouel et al. 1985; Yin and Graham 2011). Such time-dependent rates allow investigating time-delayed response of clay consolidations to p and ρ transients. We sketch the solutions for just a particularly simple case but the general case is again an open question.

Acknowledgements

We thank Prof. Carminati for help and critics, Dr. M. Sommacal for providing essential mathematical information. We also thank the two reviewers for their comments and creative suggestions about the rock deformation effects, the time-delayed clay perturbations and the natural rock heterogeneity, namely the open question described here. This work has been possible thanks to the research project PON01-02710 "MASSIMO".

Appendix A: The Structure of the Fronts

We here analyze some properties of the Burgers-like Eq. (5): this is not a formal mathematical demonstration but just an exact, intuitive sketch. Consider in general the equation

$$\frac{\partial T}{\partial t} = D\frac{\partial^2 T}{\partial z^2} + M T^2 \tag{A1}$$

with D, M constants and define $Q = \partial T/\partial z$. Equation (A1) becomes

$$\frac{\partial Q(T)}{\partial t} - D\frac{\partial^2 Q(T)}{\partial z^2} - M T^2 \frac{\partial Q(T)^2}{\partial z} - N\frac{\partial Q(T)}{\partial z} = 0 \tag{A2}$$

Assuming that $T = T_0$ is constant in a small region around $z \approx a$ and $T = T_0 + T_I$ is again constant around $z \approx b$ we thus have that $Q(a) = Q(b) = 0$ in the above small regions. In turn, a z-derivative of equation (A2) gives that in small regions around $z = a$, b one has $\frac{\partial^2 Q}{\partial z^2} = M^2\frac{\partial (Q^2)}{\partial z} = \frac{\partial Q}{\partial z} = 0$. Once integrated between a and b, the relation (A2) therefore gives

$$\int_a^b \frac{\partial Q}{\partial t}\,\mathrm{d}z = \frac{\partial}{\partial t}\int_a^b Q\,\mathrm{d}z = \frac{\partial}{\partial t}\left[T(b) - (T(a)\right] = 0 \tag{A3}$$

that implies that $T(b) - T(a) = T_0 + T_\mathrm{I} - T_0 = T_\mathrm{I} = \text{const}$.

If the solution of (A1) is growing like a polynomial z, z^2, …. in the a–b interval and we fix that $a = 0$ and $b = z_B$, to satisfy Eq. (A3) we must assume $T(z_\mathrm{B},t) = T_0 + T_I$ and just a flat $T(z, t) = T_0$ for $z > z_\mathrm{B}(t)$. This in particular implies that $T(z_\mathrm{B}) = T_0 + T_\mathrm{I}$, in the source for $t \to 0$ and $z \to 0$.

Appendix B: Estimate of the Ranges of the Equations Parameters

A quick analysis of the ranges of the available data allows to state parameter uncertainties χ, often particularly large as for the rock permeability k, a strongly pressure-dependent quantity. In addition to such $k(p)$ variability, a rather rough estimate of the other parameter variability somehow infer the order of magnitude of parameter ranges:

1. in Pierre shale k is between 10^{-16} and 10^{-20} in SI, while $\chi \approx 20\%$ for porosity and solute density.
2. in Bearpaw shale k is between 10^{-19} and 10^{-22} while for the other parameters again $\chi \approx 30\%$ for solute density and $\chi \approx 20\%$ for porosity
3. In Boom clay k is between 10^{-17} and 10^{-20} while $\chi \approx 30\%$ for porosity and solute density. The permeability uncertainties are larger than in Pierre shale.
4. for Oxnard-Mugu k is between 10^{-15} and 10^{-17}, $D \approx 10^{-5}$–10^{-8} in SI, while for the other parameters $\chi \approx 15$–30%.

In synthesis, disregarding such k variability uncertainties, one can roughly estimate $\chi \approx 15$–30% for the rock parameters.

References

Alexander, J. (1990). A review of osmotic processes in sedimentary basins. *British Geological Survey. Technical Report* WE/90/12, 76.

Appold, M. S., & Nunn, J. A. (2002). Numerical models of petroleum migration via buoyancy-driven porosity waves in viscously deformable sediments. *Geofluids, 2,* 233–247.

Baeyens, B., Maes, A., & Cremers, A. (1985). In-situ physico-chemical characterization of Boom Clay. *Radioactive Waste Management and the Nuclear Fuel Cycle, 6,* 391–408.

Barbour, S. L., & Fredlund, D. G. (1989). Mechanisms of osmotic flow and volume change in clay soils. *Canadian Geotechnical Journal, 26,* 551–562.

Bonafede, M. (1991). Hot fluid migration an efficient source of ground deformation: application to the 1982–1985 crisis at Campi Flegrei—Italy. *Journal of Volcanology and Geothermal Research, 48,* 187–198.

Bredehoeft, J. D., Neuzil, C. E. & Milly P. C. D. (1983). Regional flow in the Dakota aquifer: A study of the role of confining layers *U.S. GEOLOGICAL SURVEY WATER-SUPPLY PAPER 2237*, 45.

California Department of Water Resources, 1971.Seawater intrusion: Aquitards in the coastal groundwater basin of Oxnard Plain, Ventura Country. Calif. *Dept. of Water Resour. Bull. pp. 63–4*.

Caserta, I., Kanivesky, R. & Salusti, E. (2013). On Solitary Shock Waves for Solute and Fluid Pressure in Geologic Porous Media. In *Poromechanics*V (pp. 533–540). doi: 10.1061/9780784412992.063.

Cey, B. D., Barbour, S. L., & Hendry, M. J. (2001). Osmotic flow through a Cretaceous clay in southern Saskatchewan, Canada. *Canadian Geotechnical Journal, 38*(5), 1025–1033.

Connolly, J. A. D., & Podladchikov, Y. Y. (1998). Compaction-driven fluid flow in viscoelastic rock. *Geodinamica Acta, 11,* 55–84.

Connolly, J. A. D., & Podladchikov, Y. Y. (2014). An analytical solution for solitary porosity waves: Dynamic permeability and fluidization of nonlinear viscous and viscoplastic rock. *Geofluids.* doi:10.1111/gfl.12110.

De Cannière, P., Moors, H., Lolevier, P., De Preter, P. & Put, M. J. (1996). Laboratory and in situ migration experiments in the Boom Clay. *European Commission, Luxemburg Report*, EUR 16927.

Delage, P., Cui, Y. J., & Tang, A. M. (2010). Clays in radioactive waste disposal. *Journal of Rock Mechanics and Geotechnical Engineering., 2*(2), 111–123.

Dragila, M. I., Hay, K. M. & Wheatcraft, S. W. (2016). Initial pipe development within epikarstmicrofractures. In: Feinberg, J., Gao, Y. & Alexander, E.C., Jr., (eds.) *Caves and Karst Across Time: Geological Society of America Special Paper* (vol. 516, pp. 1–8). doi:10.1130/2016.2516(10).

Engelder, T., Cathles, L. M., & Bryndzia, L. T. (2014). The fate of residual treatment water in gas shale. *Journal of Unconventional Oil and Gas Resources, 7,* 33–48. doi:10.1016/j.juogr.2014.03.002.

Erol, O. (1977). *Clay structure and creep behavior of clays as a rate process, Thesis*, Iowa State University.

Fabre, G., & Pellet, F. (2006). Creep and time-dependent damage in argillaceous rocks. *International Journal of Rock Mechanics and Mining Sciences, 43,* 950–960.

Freeze, R. A., & Cherry, J. A. (1979). *Groundwater*. Englewood Cliffs: Prentice-Hall Inc.

Garavito, A. M., De Canniere, P., & Kooi, H. (2007). In situ chemical osmosis experiment in the Boom Clay at the Molunder ground research laboratory. *Physics and Chemistry of the Earth, 32,* 421–433.

Ghassemi, A., & Diek, A. (2003). Linear chemo-poroelasticity for swelling shales: theory and Applications. *Journal of Petroleum Science and Engineering, 38,* 199–212.

Gonçalvès, J., de Marsily, G., & Tremosa, J. (2012). Importance of thermo-osmosis for fluid flow and transport in clay formations hosting a nuclear waste repository. *Earth and Planetary Science Letters, 339–340,* 1–10. doi:10.1016/j.epsl.2012.03.032.

Greenberg, J. A., Mitchell, J., & Witherspoon, J. (1973). Coupled salt and water flows in a groundwater basin. *Journal of Geophysical Research, 78*(27), 6341–6353.

Hart, M. L. (2012). Low-head hyper filtration through Jurassic-Cretaceous metamorphic Darrington Phyllite discs (from the Northwest Cascades of Washington State, USA). *Hydrogeology Journal*. doi:10.1007/s10040-012.

Helgerud, M. B., Dvorkin, J., Nur, A., Sakai, A., & Collett, T. (1999). Effective wave velocity in marine sediments with gas hydrates: Effective medium modeling. *Geophysical Research Letters, 26,* 2021–2024.

Henrion, R., Put, M. J. & Monsecour, M. (1990). Synthesis report on transport of radionucleides in Boom Clay, state of the art.R-2863.

House, W. M. & Pritchett, J. A. (1995). Fluid migration associated with allochthonous salt in Northern Gulf of Mexico. In *4th International Congress of Brasilian Geophysical Society.*

Joshi, A., Appold, M. S., & Nunn, J. A. (2012). Evaluation of solitary waves as a mechanism for oil transport in poroelastic media: A case study of the South Eugene Island field. *Gulf of Mexico basin, Marine and Petroleum Geology, 37,* 53–69.

Kanivetsky, R., (1978). *Hydrogeologic map of Minnesota, bedrock hydrogeology, state series*, Map 2.

Kanivetsky, R. & Walton, M. (1979). *Hydrogeologic map of Minnesota, bedrock hydrogeology: A discussion to accompany state map series*, Map S-2, 11.

Kim, J. S., Kwon, S. K., Sanchez, M., & Cho, G. C. (2011). Geological storage of high level nuclear waste. *KSCE Journal of Civil Engineering, 15,* 721–737. doi:10.1007/s12205-011-0012-8.

Lerouel, S., Kabbaj, M., Tavenas, F., & Bouchard, R. (1985). Stress-strain-strain rate relation for the of sensitive natural clays compressibility. *Geotechnique, 35*(2), 159–180.

Magara, K. (1974). Compaction, ion filtration, and osmosis in shale and their significance in primary migration. *American Association of Petroleum Geologists Bulletin, 58*(2), 283–290.

Marine, I. W., & Fritz, S. J. (1981). Osmotic model to explain anomalous hydraulic heads. *Water Resources Research, 17*(1), 73–82.

Mc Tigue, D. F. (1986). Thermoelastic response of fluid-saturated rock. *Journal of Geophysical Research, 91*(89), 9533–9542.

Merlani, A., Natale, G., & Salusti, E. (2001). On the theory of pressure and temperature non-linear waves in fluid saturated porous rocks. *Geophysics and Astrophysics Fluid Dynamics, 85,* 97–128.

Merlani, A., Salusti, E., & Violini, G. (2011). Non-linear waves of fluid pressure and contaminant density in swelling shales. *Journal of Petroleum Science and Engineering, 79*(1–2), 1–9.

Natale, G., & Salusti, E. (1996). Transient solutions for temperature and pressure waves in fluid saturated porous rocks. *Geophysical Journal International, 124,* 649–654.

Neuzil, C. E. (2000). Osmotic generation of ''anomalous'' fluid pressures in geological environments. *Nature, 403*(6766), 182–184.

Neuzil, C. E., & Provost, A. M. (2009). Recent experimental data may point to a greater role for osmotic pressures in the subsurface. *Water Resources Research, 45,* W03410. doi:10.1029/2007WR006450.

Nunn, J. A. (1997). Development of geopressure by ductile shear: an example from offshore Lousiana. *Gulf Coast Association of Geological Society Transaction, 47,* 425–434.

Onsager, L. (1931). Reciprocal Relations in Irreversible Processes. I. *Physical Review, 37,* 405–426.

Rice, J. R., & Cleary, M. P. (1976). Some basic stress-diffusion solutions for fluid saturated elastic media with compressible constituents. *Reviews of Geophysics and Space Physics, 14,* 227–241.

Sarout, J., & Detournay, E. (2011). Chemoporoelastic analysis and experimental validation of the pore pressure transmission test for reactive shales. *International Journal of Rock Mechanics and Mining Sciences, 48,* 759–772.

Schlemmer, R., Friedheim, J. E., Growcock, F. B., Bloys, J. B., Headley, J. A. & Polnazsek, S. C. (2003). *Chemical osmosis, shale, and drilling fluids*. SPE 86912.SPE, 2003 Drilling and Completions Conference.

Scott, D. R., & Stevenson, D. J. (1984). Magma solitons. *Geophysical Research Letters, 11,* 1161–1164.

Shapiro, S. A., & Dinske, C. (2009). Fluid-induced seismicity: Pressure diffusion and hydraulic fracturing. *Geophysical Prospecting, 57,* 301–310. doi:10.1111/j.1365-2478.2008.00770.x.

Simm, R. (2007). Practical Gassmann substitution in sand/shale sequences. *First Break, 25,* 61–68.

Sorek, S. (1996). A model for solute transport following an abrupt pressure impact in saturated porous media. *Transport in Porous Media, 22,* 271–285.

Whitham, G. B. (1974). *Linear and nonlinear waves, pure and applied mathematics*. New York: Wiley Interscience Publication.

Wiggins, C., & Spiegelman, M. (1995). Magma migration and magmatic solitary waves in 3-D. *Geophysical Research Letters, 22,* 1289–1292.

Yin, J.-H., & Graham, J. (2011). Elastic viscoplastic modeling of time-dependent stress–strain behaviour of soils. *Canadian Geotechnical Journal, 26,* 199–209. doi:10.1139/cgj-36-4-736.

Zeynali, M. E. (2012). Mechanical and physico-chemical aspects of wellbore stability during drilling operations. *Journal of Petroleum Science and Engineering, 82–83,* 120–124. doi:10.1016/j.petrol.2012.01.006.

Zhang, J. (2011). Pore pressure prediction from well logs: Methods, modifications, and new approaches. *Earth-Science Reviews, 108,* 50–63. doi:10.1016/j.earscirev.2011.06.001.

(Received July 7, 2016, revised June 5, 2017, accepted July 25, 2017, Published online August 4, 2017)